High photon energy spectroscopy of NiO: Experiment and theory

S. K. Panda,[1,*] Banabir Pal,[2,*] Suman Mandal,[2] Mihaela Gorgoi,[3] Shyamashis Das,[2] Indranil Sarkar,[4] Wolfgang Drube,[4] Weiwei Sun,[1] I. Di Marco,[1] Andreas Lindblad,[1] P. Thunström,[5] A. Delin,[1,6,7] Olof Karis,[1] Y. O. Kvashnin,[1] M. van Schilfgaarde,[8] O. Eriksson,[1,†] and D. D. Sarma[1,2,9,‡]

[1]*Department of Physics and Astronomy, Uppsala University, Box 516, SE-751 20 Uppsala, Sweden*

[2]*Solid State and Structural Chemistry Unit, Indian Institute of Science, Bengaluru 560012, India*

[3]*Helmholtz-Zentrum Berlin für Materialien und Energie GmbH, Albert-Einstein-Str. 15, 12489 Berlin, Germany*

[4]*Deutsches Elektronen-Synchrotron DESY, Notkestrasse 85, D-22607 Hamburg, Germany*

[5]*Institute for Solid State Physics, Vienna University of Technology, 1040 Vienna, Austria*

[6]*Department of Materials and Nanophysics, School of Information and Communication Technology, Electrum 229, Royal Institute of Technology (KTH), SE-16440 Kista, Sweden*

[7]*SeRC (Swedish e-Science Research Center), KTH, SE-10044 Stockholm, Sweden*

[8]*Department of Physics, King's College London, Strand, London WC2R 2LS, United Kingdom*

[9]*Council of Scientific and Industrial Research-Network of Institutes for Solar Energy (CSIR-NISE), New Delhi 110001, India*

We have revisited the valence band electronic structure of NiO by means of hard x-ray photoemission spectroscopy (HAXPES) together with theoretical calculations using both the GW method and the local density approximation + dynamical mean-field theory (LDA+DMFT) approaches. The effective impurity problem in DMFT is solved through the exact diagonalization (ED) method. We show that the LDA+DMFT method in conjunction with the standard fully localized limit (FLL) and around mean field (AMF) double-counting alone cannot explain all the observed structures in the HAXPES spectra. GW corrections are required for the O bands and Ni-*s* and *p* derived states to properly position their binding energies. Our results establish that a combination of the GW and DMFT methods is necessary for correctly describing the electronic structure of NiO in a proper *ab initio* framework. We also demonstrate that the inclusion of photoionization cross section is crucial to interpret the HAXPES spectra of NiO. We argue that our conclusions are general and that the here suggested approach is appropriate for any complex transition metal oxide.

The electronic structure of the late 3*d* transition metal monoxides (TMO) has been studied intensely [1–17]. Despite their apparent simplicity, they exhibit a rich variety of physical properties. It is by now clear that most of these properties arise due to the strong Coulomb interaction among the 3*d* electrons of the transition metal ion.

NiO is the archetype of TMO with strong correlation effects, and has often served as the system of choice when new experimental and theoretical methods are benchmarked. The electronic structure of NiO has remained enigmatic and controversial over the decades and have also become a major topic of textbooks on condensed matter physics [3–5,18,19]. Over the years, a number of x-ray photoemission spectroscopy (XPS) and bremsstrahlung isochromat spectroscopy (BIS) studies [13,20–23] were carried out to address its electronic structure. There also have been several theoretical attempts, ranging from model approaches [3,24–27] to first-principles calculations [14,28–37], to explain different spectroscopic manifestations of NiO.

Initially, the electronic structure of NiO was interpreted using ligand field theory where the insulating gap is primarily determined by the large Coulomb interaction *U* between Ni-*d* states, an ideal case of a Mott insulator [3,18]. This interpretation, however, could not be reconciled with res-

onance photoemission experiments [38,39], since it failed to capture the right character of the multielectron satellite observed at high binding energy (around 9 eV). Later, Fujimori *et al.* [24] explained using a cluster model that the high-energy satellite arises due to the d^7 final state configuration, which was consistent with resonance photoemission results [38,39]. Based on their configuration interaction model, Sawatzky and Allen [21] also interpreted the XPS and BIS data of NiO and suggested that the fundamental gap opens between O-*p* and Ni-*d* states and is determined by Δ, the so-called charge transfer energy. A few other studies [29,35] also indicate that the first valence peak is originally a bound state coming from the strong hybridization of Ni 3*d* and O 2*p* states. This establishes NiO to be a charge transfer insulator, being, however, very close to an intermediate regime of the Zaanen-Sawatzky-Allen diagram where $U \approx \Delta$ [6].

Although the cluster approach [21,24] could explain most of the features in the experimental spectrum, it has a drawback in that it ignores the band aspects of all states, which play an important role as revealed from the angle-resolved photoemission spectroscopy (ARPES) experiments [28,29,40]. Since band dispersion is a natural ingredient in first-principles-based calculations of the electronic structure, there is a vast number of publications on NiO in this field [14,28–37]. However, the conventional effective single-particle band theory [e.g., within local (spin) density approximation—L(S)DA] has been found to fail in most aspects of the divalent transition metal oxides, such as NiO. For instance, it does in general not yield a band gap [2,41] and for NiO this approach produces much

_____

*These authors contributed equally to this work.

†olle.eriksson@physics.uu.se

‡sarma@sscu.iisc.ernet.in

smaller values of both the band gap and the local magnetic moment compared to experiment [21]. The deficiency of the DFT/L(S)DA method was partially solved by adding an orbital-dependent Hubbard U term between the localized d electrons in a mean-field fashion within the L(S)DA+ U approach [7,42]. Although the LSDA+U method [7,42] improves the values of the energy gap and local moment by a significant amount [32], this theory still fails to provide an accurate description of the electronic excitation spectra. Another theoretical approach applied to the transition metal oxides is the so-called GW approximation of Hedin [43] which also could not reproduce both XPS and BIS spectra of NiO at the same time [11,44]. This failure is most likely due to an insufficient treatment of the local correlation effects of the Ni d-orbitals, as was shown in Ref. [12]. It is also interesting to note that most of the DFT and DFT+U studies on NiO were focused on its antiferromagnetic state and, moreover, in early theoretical works the presence of an insulating gap was even attributed to the existence of long-range magnetic order [4]. However, it is known by now that NiO shows an insulating behavior even above the Néel temperature, i.e., in the absence of antiferromagnetic order [45]. This highlights the failure of any Slater-type formalism [46] in explaining the insulating behavior of NiO. More recent experiments [45,47] even suggest that long-range magnetic order has no significant influence on the valence band photoemission spectra. To overcome the limitations of the earlier methods, the electronic spectrum of the insulating PM phase of NiO has also been calculated within the recently developed LDA+DMFT scheme [48,49], which offers a more sophisticated treatment of the correlation effects. The LDA+DMFT approach successfully established that long-range AFM order has no significant influence on the valence band photoemission spectra and the large insulating gap in the PM phase is completely due to electron correlation effects [33,36]. Furthermore, the valence band spectrum of NiO calculated within LDA+DMFT agrees well with the experimentally measured spectrum recorded at 1.48-keV photon energy [33,36].

Recent experimental data [23] show that the relative intensities of the various features of the NiO valence band photoemission spectrum are very sensitive to the incident photon energy. In particular, a new feature appears at higher binding energy ($\sim$7 eV) with increasing photon energy. These observations lack an explanation. Since photoemission spectra become less surface sensitive with an increase of the incident photon energy, these new experimental data must be viewed as a better representation of the valence band spectrum of bulk NiO, compared to previous experimental results. Hence, in order to claim a detailed understanding of the valence band spectrum of NiO, and transition metal oxides in general, one must theoretically reproduce the main features of these new experiments. In view of the above, we report the experimental investigations of the valence band spectrum of NiO, to eliminate any doubts on the veracity of these new observations [23], combined with theoretical calculations, that aim to provide an understanding of measured spectroscopic features. A detailed comparison of the theoretical results with the experimental ones reveals that a combination of LDA+DMFT and GW methods, together with a proper account of the cross sections for the photoemission process, are required for describing the

experimental data. This establishes the minimal requirements for a complete theoretical framework for treating the valence band spectrum in a generic correlated oxide.

The variable energy hard x-ray photoelectron spectroscopy (HAXPES) experiments have been performed at 300 K for three different photon energies (2, 4, and 6 keV) with the photoelectron momentum parallel to the polarization vector of the light. Valence band spectra were collected at room temperature using a fixed, grazing incidence geometry ($\sim$10° grazing incidence). The base pressure in the HAXPES chamber was 1.0×10^{-9} Torr and the experiments were performed on a NiO single crystal freshly cleaved along the 100 direction before the measurements.

Our theoretical investigation is based on the LDA+DMFT [48,49] and GW [43] methods, together with the calculation of energy-dependent matrix elements of the photoemission process [50,51]. The calculations in LDA+DMFT were carried out in the paramagnetic phase by means of the RSPt code [52], based on the FP-LMTO method [53,54]. The accuracy of this method was found similar to other augmented plane-wave methods [55]. More details on this implementation can be found in Refs. [56–58]. The effective impurity problem for the Ni-3d states was solved through the exact diagonalization (ED) method, as described in Ref. [36]. Strong Coulomb repulsion between Ni-d orbitals was parametrised with $U = 8.5$ eV and J =0.8 eV. A similar value of U (8 eV) had also been used in an earlier DMFT study [33]. For the double counting correction (DCC), we used its FLL [30] and AMF [59] formulations. The calculations were carried out for a temperature of 300 K. The fitting of the hybridization function for the ED simulation was done with two bath sites for each 3d orbital. We have also carried out the quasiparticle self-consistent GW (QSGW) simulations following the implementation of Ref. [60]. In our final spectra combining the GW and DMFT, we have considered the renormalization of sp states due to the GW corrections, while no nonlocal self-energy corrections are applied to the Ni 3d states, which are well described via DMFT.

The photoemission spectra have been calculated within the single-scatterer final-state approximation [50,51]. Here the photocurrent is a sum of local (atomic-like) and partial (l-like) density of states (DOS) weighted by the corresponding cross sections. The cross sections calculated in this method depend on three quantities: the incident photon energy, the self-consistent potential and the binding energy of each state. The calculated spectra were broadened with a Gaussian to simulate the effect of spectrometer resolution.

The results of the HAXPES measurement, on a freshly cleaved NiO(100) single crystal are shown in Fig. 1. The valence band spectra of NiO at these three excitation energies are found to have several distinct features, which are marked in Fig. 1. Our measured spectrum at 2 keV shows that the most conspicuous peak (feature I) appears close to the fermi level, followed by a dip (feature II) and a small peak (feature III) around 7-eV binding energy. The multielectron satellite (feature IV) is seen around 9-eV binding energy. Interestingly, we observe that with increasing photon energy the spectral intensity of feature III is significantly enhanced and becomes the dominant peak at 6-keV photon energy. We note that the
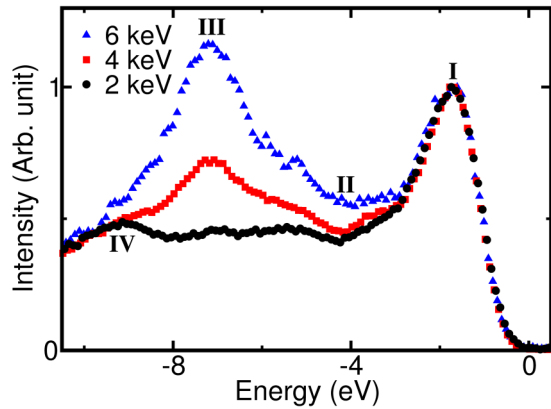
FIG. 1. HAXPES spectra of NiO valence band for three different photon energies (2, 4, and 6 keV).

earlier reported valence band XPS data [19,21] find a second Ni-d peak just after feature I at low binding energy. The absence of this structure in Fig. 1 may be attributed to the larger broadening of the present experiment. Our experimental findings are consistent with previous reports [21,23].

As described above, we first calculated the electronic structure of NiO within LDA+DMFT approaches with FLL DCC using an ED implementation, which has earlier been successful to reproduce the spectroscopic data of NiO using Al K-α photon energy (1.48 keV) [36]. The results of the present calculations, displayed in Fig. S1 of the Supplemental Materials [61], are in agreement with earlier DMFT studies [33,36]. We would like to point out here that our calculations result in strong hybridization between Ni-d and O-p states, in combination with significant many-electron features of the Ni $3d$ shell. In addition, we find a substantial amount of Ni-s-, O-s-, and Ni-p-like states, located at binding energies that roughly coincide with feature III in Fig. 1. The calculated

band gap ($\sim$2.7 eV), obtained with the FLL DCC is found to be smaller compared to the experimental value ($\sim$4 eV) [21]. Such an underestimation of the insulating gap can be attributed to the error associated with the standard combination of full charge self-consistency and the FLL double-counting procedure as has been discussed in Ref. [62]. However, upon changing the DCC scheme to AMF, the magnitude of the gap becomes about 4 eV, which is in good agreement with the experimental value [21]. This establishes that the LDA+DMFT in conjunction with the AMF DCC provides a more accurate estimation of the band gap of NiO. Our results also reveal that the splitting between O-p and Ni-d levels is larger for AMF than FLL DCC. We will see below that this enhancement of the d-p splitting has important consequences in explaining the HAXPES data.

Next, we computed the photoemission spectra as described above and compared to our measurements. As we can see in Fig. 2(a), our computed spectra with both the DCC reproduce most features of the experimental HAXPES data for the three photon energies, both the peak at the top of the valence band, as well as the increased intensity of feature III, with increasing photon energy. The photon energy governed enhancement of the intensity of feature III is found to be due to an increase of the cross section of the states around 6- to 7-eV binding energy, for the experiments that use a higher photon energy. To illustrate this clearly, we first analyze the FLL results. The corresponding spectral intensities of l-projected states are shown in Fig. 2(b). The contribution from O-p states is very small throughout the entire energy range due to the low cross section of these states. Our calculations further show that the sharp peak near the Fermi level (feature I) has always a predominant Ni-d character for all probed photon energies. However, the multielectron satellite (feature IV) observed around 9-eV binding energy is not only due to the Ni-d states, but has almost equal contribution from the O-s states for the 2- and 4-keV photon energies. When we increase the photon
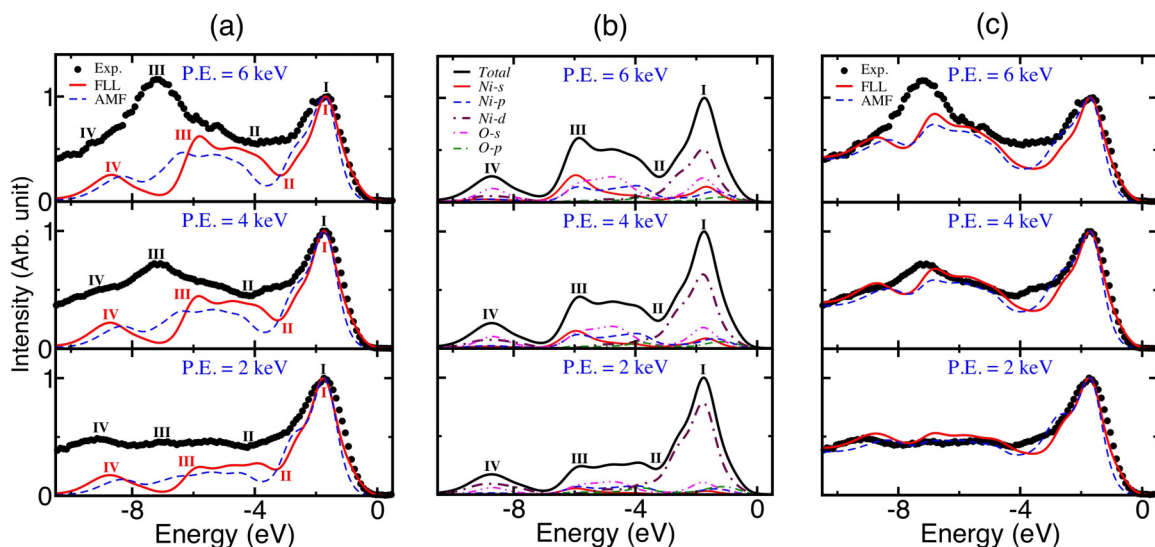
FIG. 2. (a) A comparison of our computed spectra from LDA+DMFT results with the measured HAXPES data. (b) Spectral intensities of all the Ni and O l projected states to the total spectra are shown. (c) A comparison of our computed spectra after incorporating the GW corrections and the background effects with the measured data. The results corresponding to FLL and AMF DCC are shown in (a) and (c), while only FLL results are displayed in (b).

energy to 6 keV, the O-*s* contribution dominates [see Fig. 2(b)]. The spectral intensity around feature III is found to originate from the cumulative contribution from Ni-*s*, Ni-*p*, and O-*s* states for all photon energies. The most significant contribution to this peak comes from the Ni-*s* states whose relative cross section is higher in magnitude as compared with the other states (primarily Ni-*d*) and increases rapidly with increasing photon energy. This gives rise to a sharp enhancement of the spectral weight of these states, at higher photon energies. We note that this is also true for the AMF results. However, the feature III in AMF appears at about 0.5 eV higher binding energy [see Fig. 2(a)] than FLL, providing a better agreement with the experimental data. This implies that the positions of the delocalized *s* and *p* states are better described with AMF than FLL DCC. The quantitatively wrong estimations of the relative positions of the *sp* states within LDA+DMFT with conventional FLL DCC was also found by Dang and coworkers [62,63] and a remedy was suggested by adjusting the double counting potential using a different value of *U* for its evaluation [64]. In this context, it was also shown [65] that for a fixed correlation strength the distance between the *d*- and *p*-dominated peaks is governed only by the occupancy (N_d) of the *d* orbital. Our charge self-consistent results in $N_d = 8.17$ and $N_d = 8.07$ for FLL and AMF DCC, respectively. Thus, the enhanced *d*-*p* splitting in our AMF result is consistent with Ref. [65].

As discussed above, features II and III are shifted toward the right direction by changing the DCC from FLL to AMF. However, in both cases they still appear at lower binding energies, compared to the experiment. Although the LDA+DMFT method can in principle be applied to include local correlation effects for any type of orbitals, including the *sp* states, finding a proper *U* parameter would be problematic in this case. Moreover, the nonlocal correlations usually play a more important role for delocalized orbitals. The GW method is constructed to describe nonlocal correlation effects within a fully *ab initio* approach and without additional parameters. Its accuracy can be evidenced by comparing theoretical and experimental values of the band gap in *sp*-bonded systems [66]. An already published GW study [37] of NiO indicates that the positions of *s*- and *p*-derived states are shifted toward higher binding energy, compared to results obtained from LDA. To explore this as a possible explanation for the difference in calculated and measured positions of features II and III in Fig. 2, we carried out a quasiparticle fully self-consistent GW calculation [60]. The results of our calculations are shown in Fig. S2 of the Supplemental Material [61]. A comparison of the QSGW and DMFT results, as discussed in the Supplemental Material [61], clearly reveals that QSGW pushes the *sp* peaks around 6 eV toward higher binding energy, making the bandwidth larger compared to the DMFT bandwidth of those states. The size of these effects may appear large at first, on the same scale of the correlation effects for *d*-derived states. This is surprising, since traditionally it was always assumed that the Ni-3*d* states are the crucial states to be localized. However, these results are not only the outcome of the most modern GW calculations but also consistent with a recent study [67] of the electron localization function (ELF) in CuO, which shows that the largest error due to the electron confinement in CuO is located at the O sites. We considered

the renormalization of *sp* states due to the GW corrections for the DMFT calculations. The amount of renormalizations for both the DCCs are guided by the Fig. S2 of the Supplemental Material [61]. Hence, we obtained an electronic structure that both contained effects of strong correlations of the *d* shell as well as nonlocal correlations of *sp*-derived states. After multiplication with appropriate cross sections and adding a background contribution, we obtained the final spectra that are displayed in Fig. 2(c). The background contribution was included to facilitate a direct comparison to experimental data that do contain a background due to secondary electrons. The agreement between the theoretical and experimental spectra shown in Fig. 2(c) is good for all photon energies for both the DCC schemes. This applies to the positions of the different features, as well as their relative intensities.

Although a small disagreement in the intensity distribution at 6-keV photon energy can be noticed, we observe that the intensity difference between the features II and III is correctly obtained in our calculations when comparing to the corresponding experimental data. A more elaborate discussion to show the importance of matrix elements and GW corrections in order to interpret the experimental HAXPES data for each photon energy is provided in the Supplemental Material [61] (Fig. S3).

In conclusion, our detailed experimental and theoretical study reveals that the LDA+DMFT method with FLL double counting correction as is widely used for understanding the electronic structure of strongly correlated systems, is not fully capable of interpreting the spectroscopic HAXPES data of NiO, particularly the features arising from the *s*- and *p*-derived states. We find that the positions of those features are better described through AMF DCC, but still do not agree with the experimental results. A detailed analysis shows that the GW corrections are important to properly position the binding energies of those delocalized *s*- and *p*-derived states, while DMFT properly describes the *d* states. Our analysis thus indicates that a method combining GW and DMFT techniques [68,69] is the method of choice in describing the electronic structure of NiO and most likely any complex transition metal oxide. Our results also show that the matrix element effects, which are often ignored, play a crucial role in understanding the electronic spectrum across a large range of photon energies. Therefore, with the theoretical framework outlined in this manuscript, we can successfully reproduce all features of the valence band of NiO, including the high binding energy feature, which becomes most prominent at large photon energies. Thus, the present study provides a very extensive analysis of the valence band electronic structure of NiO and most importantly suggests routes for further theoretical analysis of the valence band spectrum of the transition metal oxides.

[1] N. F. Mott and R. Peierls, Proc. Phys. Soc. London **49**, 72 (1937).

[2] L. F. Mattheiss, Phys. Rev. B **5**, 290 (1972).

[3] B. Brandow, Adv. Phys. **26**, 651 (1977).

[4] K. Terakura, A. R. Williams, T. Oguchi, and J. Kübler, Phys. Rev. Lett. **52**, 1830 (1984).

[5] K. Terakura, T. Oguchi, A. R. Williams, and J. Kübler, Phys. Rev. B **30**, 4734 (1984).

[6] J. Zaanen, G. A. Sawatzky, and J. W. Allen, Phys. Rev. Lett. **55**, 418 (1985).

[7] V. I. Anisimov, J. Zaanen, and O. K. Andersen, Phys. Rev. B **44**, 943 (1991).

[8] M. Takahashi and J.-i. Igarashi, Phys. Rev. B **54**, 13566 (1996).

[9] M. Imada, A. Fujimori, and Y. Tokura, Rev. Mod. Phys. **70**, 1039 (1998).

[10] B. Dai, K. Deng, J. Yang, and Q. Zhu, J. Chem. Phys. **118**, 9608 (2003).

[11] S. V. Faleev, M. van Schilfgaarde, and T. Kotani, Phys. Rev. Lett. **93**, 126406 (2004).

[12] S. Kobayashi, Y. Nohara, S. Yamamoto, and T. Fujiwara, Phys. Rev. B **78**, 155112 (2008).

[13] M. Taguchi, M. Matsunami, Y. Ishida, R. Eguchi, A. Chainani, Y. Takata, M. Yabashi, K. Tamasaku, Y. Nishino, T. Ishikawa, Y. Senba, H. Ohashi, and S. Shin, Phys. Rev. Lett. **100**, 206401 (2008).

[14] C. Rödl, F. Fuchs, J. Furthmüller, and F. Bechstedt, Phys. Rev. B **79**, 235114 (2009).

[15] E. Engel and R. N. Schmid, Phys. Rev. Lett. **103**, 036404 (2009).

[16] H. Jiang, R. I. Gomez-Abal, P. Rinke, and M. Scheffler, Phys. Rev. B **82**, 045108 (2010).

[17] R. Eder, Phys. Rev. B **91**, 245146 (2015).

[18] N. F. Mott, Proc. Phys. Soc. London, Sect. A **62**, 416 (1949).

[19] S. Hüfner, *Photoelectron Spectroscopy: Principles and Applications*, 3rd ed. (Springer, Berlin, 2003).

[20] D. E. Eastman and J. L. Freeouf, Phys. Rev. Lett. **34**, 395 (1975).

[21] G. A. Sawatzky and J. W. Allen, Phys. Rev. Lett. **53**, 2339 (1984).

[22] G. van der Laan, J. Zaanen, G. A. Sawatzky, R. Karnatak, and J.-M. Esteva, Phys. Rev. B **33**, 4253 (1986).

[23] J. Weinen, T. Koethe, C. Chang, S. Agrestini, D. Kasinathan, Y. Liao, H. Fujiwara, C. Schüßler-Langeheine, F. Strigari, T. Haupricht, G. Panaccione, F. Offi, G. Monaco, S. Huotari, K.-D. Tsuei, and L. Tjeng, J. Electron Spectrosc. Relat. Phenom. **198**, 6 (2015).

[24] A. Fujimori and F. Minami, Phys. Rev. B **30**, 957 (1984).

[25] M. R. Norman and A. J. Freeman, Phys. Rev. B **33**, 8896 (1986).

[26] D. D. Sarma, J. Solid State Chem. **88**, 45 (1990).

[27] G. J. M. Janssen and W. C. Nieuwpoort, Phys. Rev. B **38**, 3449 (1988).

[28] Z.-X. Shen, C. K. Shih, O. Jepsen, W. E. Spicer, I. Lindau, and J. W. Allen, Phys. Rev. Lett. **64**, 2442 (1990).

[29] Z.-X. Shen, R. S. List, D. S. Dessau, B. O. Wells, O. Jepsen, A. J. Arko, R. Barttlet, C. K. Shih, F. Parmigiani, J. C. Huang, and P. A. P. Lindberg, Phys. Rev. B **44**, 3604 (1991).

[30] V. I. Anisimov, I. V. Solovyev, M. A. Korotin, M. T. Czyżyk, and G. A. Sawatzky, Phys. Rev. B **48**, 16929 (1993).

[31] V. I. Anisimov, P. Kuiper, and J. Nordgren, Phys. Rev. B **50**, 8257 (1994).

[32] O. Bengone, M. Alouani, P. Blöchl, and J. Hugel, Phys. Rev. B **62**, 16392 (2000).

[33] X. Ren, I. Leonov, G. Keller, M. Kollar, I. Nekrasov, and D. Vollhardt, Phys. Rev. B **74**, 195114 (2006).

[34] T. Kotani and M. van Schilfgaarde, J. Phys. Condens. Matter **20**, 295214 (2008).

[35] J. Kuneš, V. I. Anisimov, S. L. Skornyakov, A. V. Lukoyanov, and D. Vollhardt, Phys. Rev. Lett. **99**, 156404 (2007).

[36] P. Thunström, I. Di Marco, and O. Eriksson, Phys. Rev. Lett. **109**, 186401 (2012).

[37] S. Das, J. E. Coulter, and E. Manousakis, Phys. Rev. B **91**, 115105 (2015).

[38] S. J. Oh, J. W. Allen, I. Lindau, and J. C. Mikkelsen, Phys. Rev. B **26**, 4845 (1982).

[39] O. Tjernberg, S. Söderholm, U. O. Karlsson, G. Chiaia, M. Qvarford, H. Nylén, and I. Lindau, Phys. Rev. B **53**, 10372 (1996).

[40] Z. X. Shen, P. A. P. Lindberg, C. K. Shih, W. E. Spicer, and I. Lindau, Physica C **162-164**, 1311 (1989).

[41] T. Cai, H. Han, Y. Yu, T. Gao, J. Du, and L. Hao, Physica B (Amsterdam) **404**, 89 (2009).

[42] F. López-Aguilar and J. Costa-Quintana, Phys. Status Solidi B **123**, 219 (1984).

[43] L. Hedin, Phys. Rev. **139**, A796 (1965).

[44] F. Aryasetiawan and O. Gunnarsson, Phys. Rev. Lett. **74**, 3221 (1995).

[45] O. Tjernberg, S. Söderholm, G. Chiaia, R. Girard, U. O. Karlsson, H. Nylén, and I. Lindau, Phys. Rev. B **54**, 10245 (1996).

[46] J. C. Slater, Phys. Rev. **82**, 538 (1951).

[47] W. Jauch and M. Reehuis, Phys. Rev. B **70**, 195121 (2004).

[48] A. I. Lichtenstein and M. I. Katsnelson, Phys. Rev. B **57**, 6884 (1998).

[49] A. Georges, G. Kotliar, W. Krauth, and M. J. Rozenberg, Rev. Mod. Phys. **68**, 13 (1996).

[50] H. Winter, P. J. Durham, and G. M. Stocks, J. Phys. F **14**, 1047 (1984).

[51] J. Redinger, P. Marksteiner, and P. Weinberger, Z. Phys. B **63**, 321 (1986).

[52] J. M. Wills, O. Eriksson, M. Alouni, and D. L. Price, *Electronic Structure and Physical Properties of Solids: The Uses of the LMTO Method* (Springer-Verlag, Berlin, 2000).

[53] O. K. Andersen, Phys. Rev. B **12**, 3060 (1975).

[54] J. M. Wills and B. R. Cooper, Phys. Rev. B **36**, 3809 (1987).

[55] K. Lejaeghere *et al.*, Science **351**, aad3000 (2016).

[56] A. Grechnev, I. Di Marco, M. I. Katsnelson, A. I. Lichtenstein, J. Wills, and O. Eriksson, Phys. Rev. B **76**, 035107 (2007).

[57] I. Di Marco, J. Minár, S. Chadov, M. I. Katsnelson, H. Ebert, and A. I. Lichtenstein, Phys. Rev. B **79**, 115111 (2009).

[58] O. Grånäs, I. Di Marco, P. Thunström, L. Nordström, O. Eriksson, T. Björkman, and J. Wills, Comput. Mater. Sci. **55**, 295 (2012).

[59] M. T. Czyżyk and G. A. Sawatzky, Phys. Rev. B **49**, 14211 (1994).

[60] T. Kotani, M. van Schilfgaarde, and S. V. Faleev, Phys. Rev. B **76**, 165106 (2007).

[61] See Supplemental Material at http://link.aps.org/supplemental/10.1103/PhysRevB.93.235138 for LDA+DMFT, QSGW spectral functions and for a detailed discussion on matrix element effects and GW corrections.

[62] H. T. Dang, A. J. Millis, and C. A. Marianetti, Phys. Rev. B **89**, 161113 (2014).

[63] H. T. Dang, X. Ai, A. J. Millis, and C. A. Marianetti, Phys. Rev. B **90**, 125114 (2014).

[64] H. Park, A. J. Millis, and C. A. Marianetti, Phys. Rev. B **90**, 235103 (2014).

[65] X. Wang, M. J. Han, L. de' Medici, H. Park, C. A. Marianetti, and A. J. Millis, Phys. Rev. B **86**, 195136 (2012).

[66] M. van Schilfgaarde, T. Kotani, and S. Faleev, Phys. Rev. Lett. **96**, 226402 (2006).

[67] F. Hao, R. Armiento, and A. E. Mattsson, J. Chem. Phys. **140**, 18A536 (2014).

[68] S. Biermann, F. Aryasetiawan, and A. Georges, Phys. Rev. Lett. **90**, 086402 (2003).

[69] J. M. Tomczak, M. Casula, T. Miyake, F. Aryasetiawan, and S. Biermann, Europhys. Lett. **100**, 67001 (2012).